Enhancement of ultracold molecule formation by local control in the nanosecond regime

New Journal of Physics

The open access journal at the forefront of physics

CrossMark

PAPER

Enhancement of ultracold molecule formation by local control in the nanosecond regime

J L Carini[1], S Kallush[2], R Kosloff[3] and P L Gould[1]

1   Department of Physics, University of Connecticut, Storrs, Connecticut 06269, USA
2   Department of Physics, ORT-Braude College, PO Box 78, 21982 Karmiel, Israel
3   Department of Physical Chemistry and the Fritz Haber Research Center for Molecular Dynamics, Hebrew University of Jerusalem, Jerusalem 91904, Israel

E-mail: phillip.gould@uconn.edu

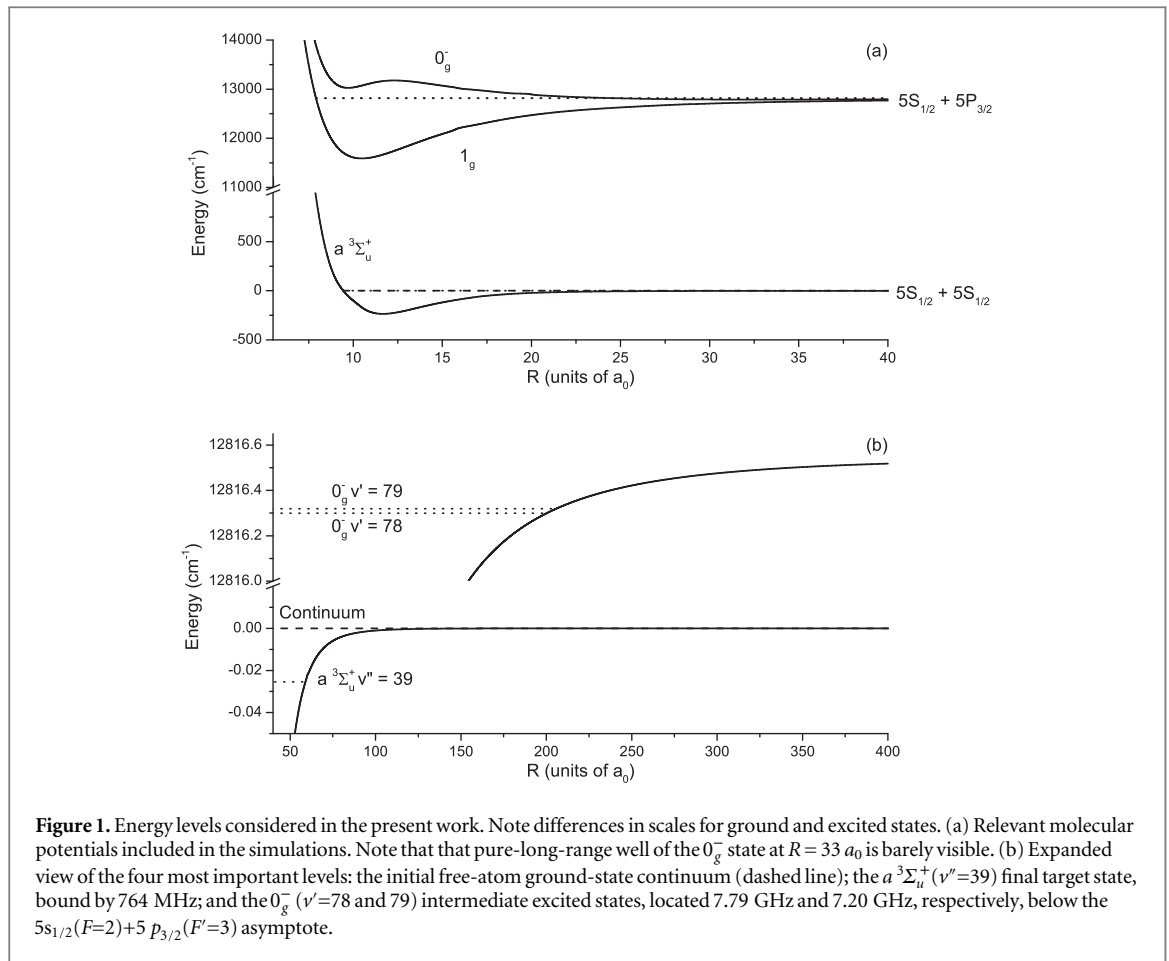**Keywords:** ultracold molecules, photoassociation, quantum control, coherent control

Abstract

We describe quantum simulations of ultracold $^{87}Rb_2$ molecule formation using photoassociation (PA) with nanosecond-time-scale pulses of frequency chirped light. In particular, we compare the case of a linear chirp to one where the frequency evolution is optimized by local control (LC) of the phase, and find that LC can provide a significant enhancement. The resulting optimal frequency evolution corresponds to a rapid jump from the PA absorption resonance to a downward transition to a bound level of the lowest triplet state. We also consider the case of two frequencies and investigate interference effects. The assumed chirp parameters should be achievable with nanosecond pulse shaping techniques and are predicted to provide a significant enhancement over recent experiments with linear chirps.

1. Introduction

Following in the footsteps of ultracold atoms, molecules at ultralow energies have generated significant excitement in recent years [1]. Applications in precision spectroscopy, quantum information processing, many-body dipolar systems, as well as investigations of chemistry at ultracold temperatures, all stand to benefit from enhanced production efficiency and improved manipulation of ultracold molecules. There are two general methods for their production: reducing the temperature of already-existing molecules; or assembling the molecules from their precooled constituent atoms. In the latter case, ultracold photoassociation (PA) [2–5] is an important example. Here, two ultracold atoms collide in the presence of laser light tuned to excite from the low-energy continuum to a bound excited state of the diatomic molecule. The atom pair undergoes a free-to-bound transition and the resulting excited molecule can subsequently decay, via incoherent spontaneous emission, into a bound level of the ground state. Since this decay is not controlled, and typically populates the states of interest with low probability, there is interest in employing the techniques of quantum control in order to increase the efficiency of photoassociative molecule formation [6].

Quantum control [7, 8] is based on employing interfering pathways to enhance an objective such as molecular formation. This type of control has been suggested as a means of manipulating ultracold collisions to enhance PA yield [9–21], stabilizing the final bound-state populations [22], and enhancing the amplitude at short internuclear distances prior to the PA step [23]. Another control objective has been to cool or concentrate molecular vibrations into a single state [24]. Experimental attempts to apply ultrafast control to the formation of ultracold molecules have so far been unsuccessful, although destruction of already existing molecules with shaped pulses has been realized [25, 26]. This lack of success is likely due to the mismatch between the timescales of the molecular system and the applied field.

The global objective of control is achieved theoretically by an iterative process, which is implemented by solving optimal control theory (OCT) equations. Local control (LC) [27–31] is a simpler unidirectional and noniterative time propagation scheme which adjusts the field at each instant of time in order to optimize the

Figure 1. Energy levels considered in the present work. Note differences in scales for ground and excited states. (a) Relevant molecular potentials included in the simulations. Note that that pure-long-range well of the 0_g^- state at $R = 33\ a_0$ is barely visible. (b) Expanded view of the four most important levels: the initial free-atom ground-state continuum (dashed line); the $a\ ^3\Sigma_u^+(v''=39)$ final target state, bound by 764 MHz; and the 0_g^- ($v'=78$ and 79) intermediate excited states, located 7.79 GHz and 7.20 GHz, respectively, below the $5s_{1/2}(F=2) + 5\ p_{3/2}(F'=3)$ asymptote.

target at the next time step. The success of LC depends crucially on the choice of the local objective. Therefore, in some cases, adjustment of the target throughout the evolution, based on knowledge of the system dynamics, can be advantageous. Normally, LC is realized via control of the amplitude. However, in order to emulate experimental capabilities, in the present work, we fix the pulse amplitude and utilize control of the phase.

To date, most of the calculational efforts involving the application of quantum control to ultracold molecule formation have involved ultrafast time scales and deeply-bound vibrational levels [6]. In contrast, we recently explored, both experimentally and theoretically, the production of ultracold molecules on slower time scales and in high vibrational levels [32]. Using 40 ns pulses of frequency-chirped light, we found evidence for coherent effects, specifically a significant dependence on the direction of the linear chirp. In the present paper, we extend our previous quantum calculations to somewhat faster time scales, and more importantly, incorporate LC of the phase in order to optimize the formation of ground-state molecules. We find that this type of quantum control, either with one frequency or two simultaneous frequencies, can indeed enhance the molecular production. The experimental realization of these controlled pulses should be possible.

The system we examine here is that utilized in our recent experiments [32] and shown in figure 1: photoassociative production of $^{87}\mathrm{Rb}_2$ in the $v'=78$ and $v'=79$ vibrational levels of the 0_g^- state just below the $5s_{1/2} + 5p_{3/2}$ asymptote. These states give efficient PA [33] since their outer turning points are at long range. The target state, which is ultimately detected, is the barely-bound $v''=39$ level of the $a\ ^3\Sigma_u^+$ lowest-lying triplet potential. In the recent experiments, we found evidence for coherent effects. The calculations showed that stimulated emission from the excited state to the target state, occurring later in the positive chirp, was responsible for the majority of the difference in molecular formation rates when using positive versus negative chirps. In the present paper, we use 15 ns pulses and numerically explore a variety of time-dependent frequencies (or phases) of the laser field.

The paper is organized as follows. In section 2, we provide more details on the system and its parameters, discuss the calculational techniques, and briefly describe LC theory and its use in controlling the phase. In section 3, we present results of the simulations, including a comparison of one frequency and two simultaneous frequencies, as well as a discussion of interference effects. Section 4 comprises concluding remarks.

2. Theoretical model with LC of the phase

The model of the PA process is taken to be similar to [32]. The ground $a^3\Sigma_u^+$ triplet state and the two 0_g^- and 1_g excited electronic states are considered according to [33] and denoted by $j = g$, e_0, and e_1, respectively. The dressed state Hamiltonian that includes the nuclear and electronic degrees of freedom is given by:

$$\hat{H} = \hat{H}_0 + \hat{H}_\epsilon = \begin{pmatrix} \hat{H}_g & 0 & 0 \\ 0 & \hat{H}_{e_0} & 0 \\ 0 & 0 & \hat{H}_{e_1} \end{pmatrix} + \begin{pmatrix} 0 & \hbar\hat{\Omega}_0(t) & \hbar\hat{\Omega}_1(t) \\ \hbar\hat{\Omega}_0^*(t) & 0 & 0 \\ \hbar\hat{\Omega}_1^*(t) & 0 & 0 \end{pmatrix}. \tag{1}$$

Here $\hat{H}_j$ is the field-free Hamiltonian for the electronic state j, the coupling between the states is given by the Rabi frequency $\hat{\Omega}_j = \mu_{gj}\epsilon(t)$, μ_{gj} are the transition dipole matrix elements between vibrational states including the Franck–Condon overlap, and $\epsilon(t)$ is the time dependent electric field:

$$\epsilon(t) = \epsilon_0 \exp\left[-\frac{(t - t_{\text{center}})^2}{2\sigma^2} + i\tilde{\omega}(t)(t - t_{\text{center}}) \right], \tag{2}$$

where ϵ_0 is the peak electric field, t_{center} is the center time of the pulse, σ is the pulse temporal width, and $\tilde{\omega}$ is the instantaneous frequency offset. As described in [32], the basis sets used in the time-dependent calculations are obtained by diagonalizing the Hamiltonian on a mapped Fourier grid [34]. They span bandwidths of ~ 15 GHz for the 0_g^- state (v'=67 to 87), ~ 15 GHz for the 1_g state (v'=217 to 239), 278 GHz for the $a^3\Sigma_u^+$ bound-state manifold (v''=30 to 40), and 16 MHz (0.77 mK) for the $a^3\Sigma_u^+$ continuum. As in [32], we ignore the contributions from the $a^3\Sigma_u^+$ (v''=40) level since it is bound by only 39 MHz and thus easily photodissociated by the chirped light. The sum over partial waves and accounting for the thermal ensemble at an assumed temperature of 150 μK are discussed in [32]. Spontaneous decay is modeled [32, 35] by adding a sink channel for each decay path from the various excited-state (0_g^- and 1_g) vibrational levels into bound states or the continuum of $a^3\Sigma_u^+$. These individual channel decay rates are determined by the excited-state lifetimes [36, 37], 26.2 ns for 0_g^- and 22.8 ns for 1_g, and the Franck–Condon factors. Although this sink-channel model precludes the possibility of multiple incoherent excitations during the pulse, its use is justified because only a small fraction (10^{-4} for 0_g^-(v'=78)) of spontaneous decays populates the target state, and this occurs mainly after the pulse.

The goal of this work is to use the ability to modulate the instantaneous field frequency $\tilde{\omega}(t)$ to optimize the formation of bound molecules in the ground state, without changing the amplitude. This usually corresponds to a projection operator into some desired bound state within the ground (target) electronic state.

Due to the narrow feasible bandwidth and limited response time of the experimental $\tilde{\omega}$, the computed control field should have a relatively simple structure with a clear mechanism in order to make it experimentally acceptable. Moreover, the relatively heavy computational load for the simulation of the dynamics demands a noniterative method, and to this point the unidirectional LC method is used. Due to its simple structure, LC results in control fields that are more directly meaningful mechanistically and, as a result, also transferable into experimentally feasible pulses.

Within the LC approach, the goal is a maximization of a target operator $\hat{P}$, which usually corresponds to a projection operator into some desired state. The time dependence of the expectation value $\langle \hat{P} \rangle$ is given by:

$$\frac{d\langle \hat{P} \rangle}{dt} = \frac{1}{i\hbar}\left\langle [\hat{P}, \hat{H}] \right\rangle + \left\langle \frac{\partial \hat{P}}{\partial t} \right\rangle = \frac{i}{\hbar}\left\langle [\hat{H}_\epsilon, \hat{P}] \right\rangle_\Psi, \tag{3}$$
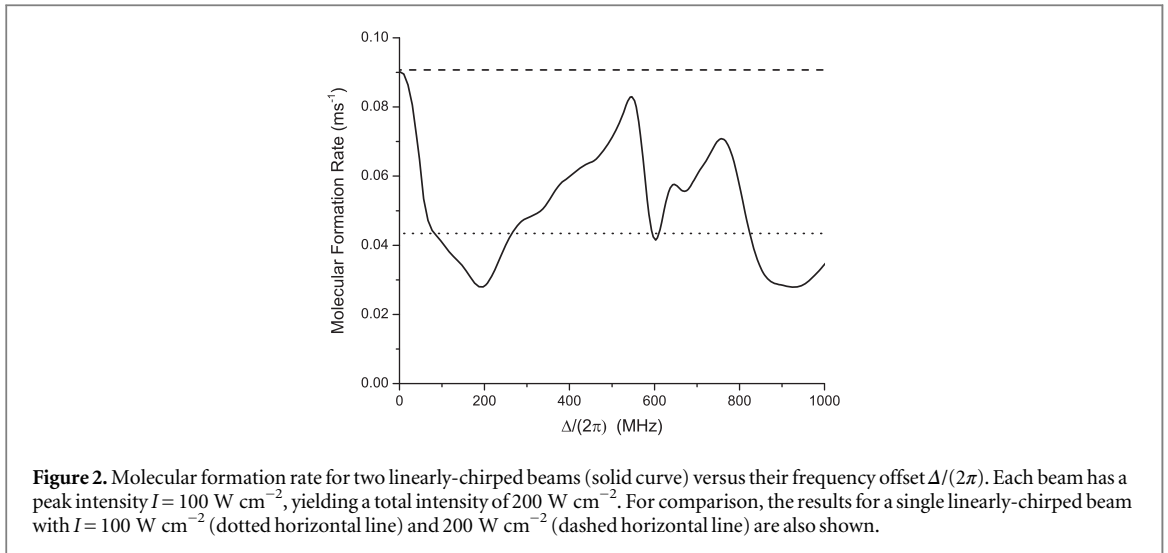
where the fact that the target state is an eigenstate of $\hat{H}_0$ is used in the last relation. Note that targeting a time-dependent goal [38] could also be easily incorporated into LC by utilizing the third term in equation (3). Inserting equation (3) into equation (1) gives:

$$\frac{d\langle \hat{P} \rangle}{dt} = -\frac{1}{2}\sum_k \Im\left\{ \hat{\Omega}_{kt}\langle \hat{P} \rangle_{gk} \right\} = -2\epsilon_0 e^{-\frac{(t - t_{\text{center}})^2}{2\sigma^2}}\sum_k \tilde{\mu}_{gk}B_k \sin\left(\varphi_k + \tilde{\omega}(t)(t - t_{\text{center}}) \right), \tag{4}$$

where the index k denotes the intermediate level, $\hat{\Omega}_{kt}$ is its coupling to the target state, and $\langle \hat{P} \rangle_{gk} \equiv B_k \exp(i\varphi_k)$ is the matrix element of $\hat{P}$ over the initial ground state wave function and the state k. The goal of the control is therefore to adjust the temporal phase of the field $\tilde{\omega}(t)$ to maintain a monotonic increase of the projection into the target state. We note that a similar application of OCT for the same goal with a given target time will give a similar condition to equation (4). The difference would be that the matrix element $\langle \hat{P} \rangle_{gk}$ will be obtained

Figure 2. Molecular formation rate for two linearly-chirped beams (solid curve) versus their frequency offset $\Delta/(2\pi)$. Each beam has a peak intensity $I = 100$ W cm^{-2}, yielding a total intensity of 200 W cm^{-2}. For comparison, the results for a single linearly-chirped beam with $I = 100$ W cm^{-2} (dotted horizontal line) and 200 W cm^{-2} (dashed horizontal line) are also shown.
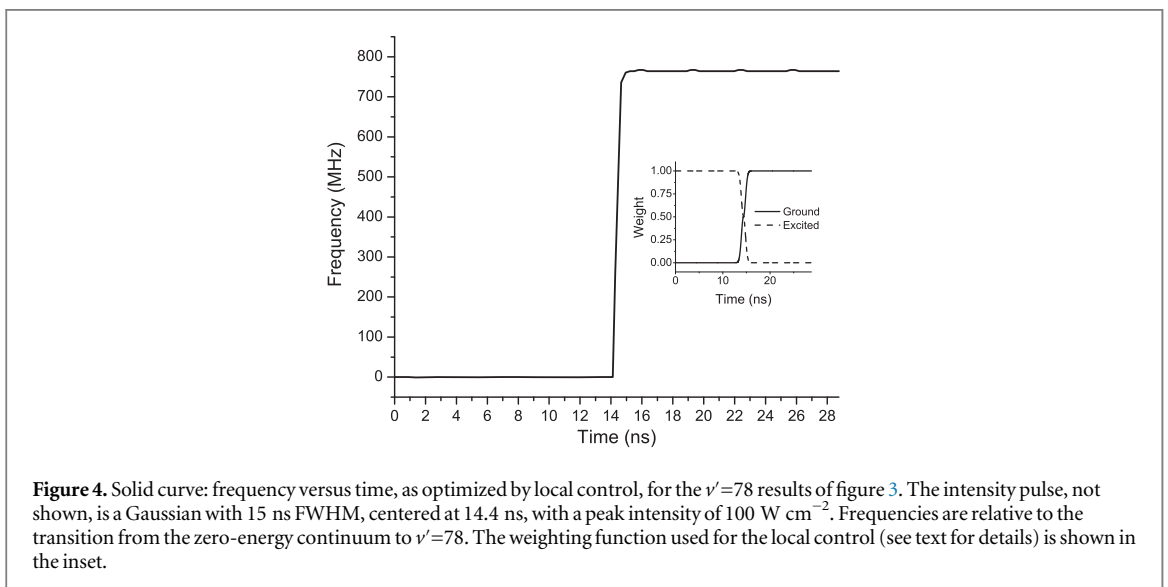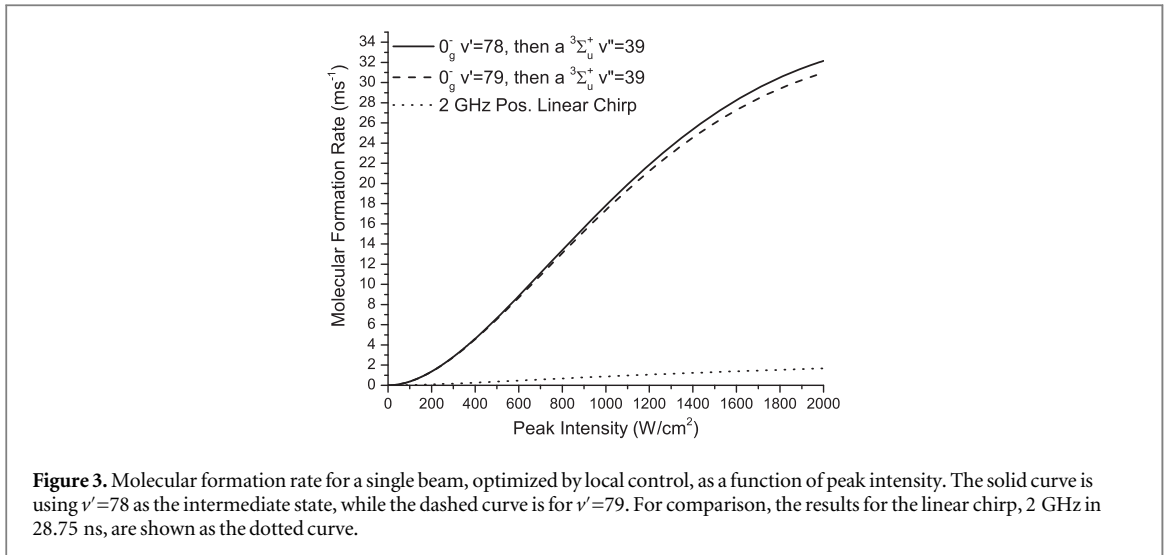
between the initial ground state and the intermediate state which was obtained by backward propagation from the target state [30].

Note that the coupling structure (equation (1)), does not allow a direct dipole transition between the initial scattering state and the target state. Commonly in LC applications, this situation leads to erratic and less efficient fields, which could be remedied by significant seeding of the intermediate state in the early stages of the control. To achieve this, we add a seeding step into the control formalism. This is done by defining a switch for the target, which will coincide with the intermediate level(s) initially and will move gradually to the final target later in the pulse, as detailed in the next section.
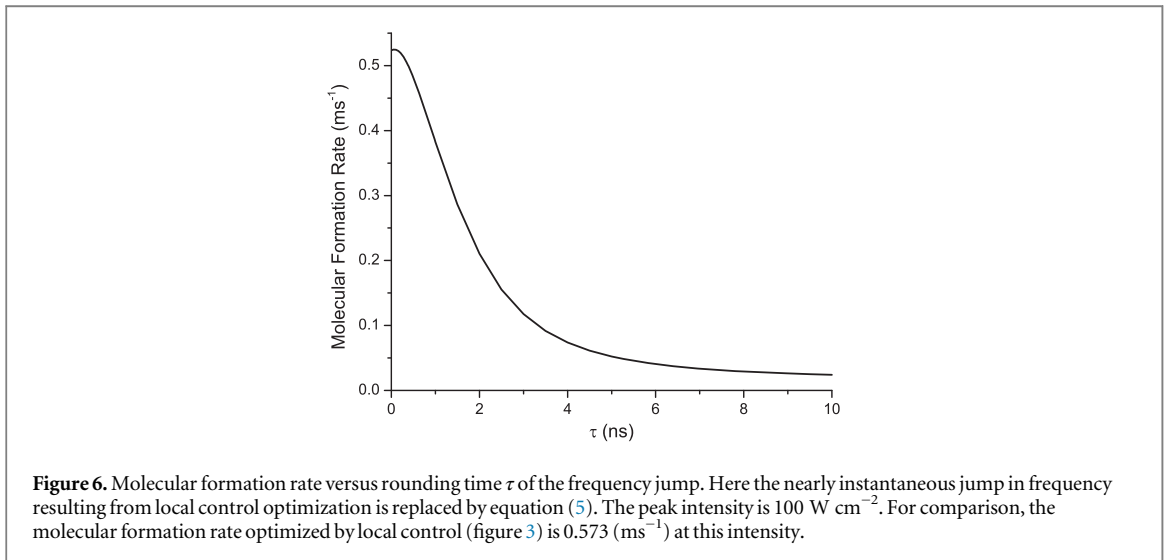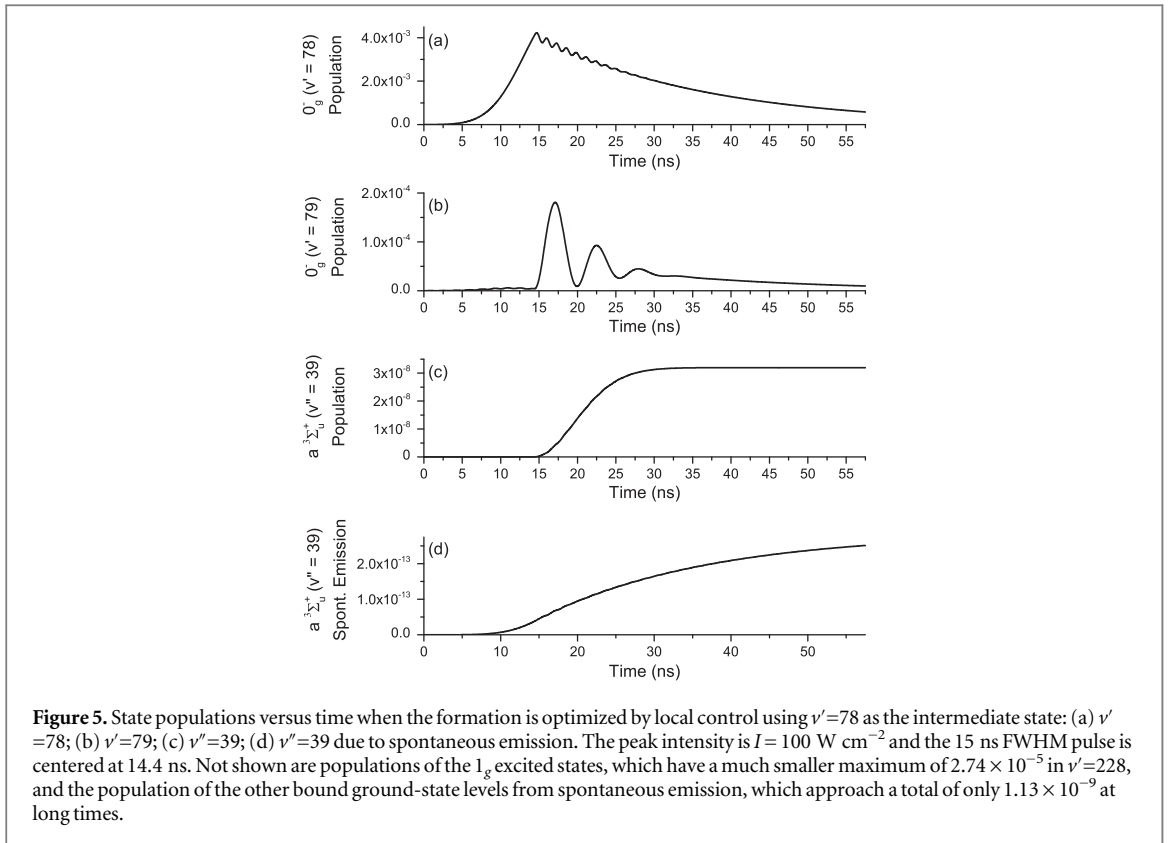
3. Results

The interpretation, based on quantum calculations, of our recent experiments [32] on frequency-chirped molecular formation was that stimulated emission from the $0_g^-(v'=78)$ excited state to the $a\,^3\Sigma_u^+(v''=39)$ target state, occurring later in the positive chirp, enhanced the formation for this chirp direction. Several possibilities come to mind for further enhancement. Employing shorter pulses and faster chirps will reduce the effects of incoherent spontaneous emission of the 0_g^- state, whose radiative lifetime is 26.2 ns [36, 37]. We have incorporated this in the present calculations, using 15 ns full-width-half-maximum (FWHM) Gaussian intensity pulses (versus 40 ns in the recent experiments) and 28.75 ns linear chirps (versus 100 ns). Also, for the linear chirp of 1 GHz in 100 ns utilized in the experiments, the frequency difference of 764 MHz between the absorption to the excited state and the stimulated emission to the target state meant that if the first step were resonant at the peak of the pulse, then the second step would occur at relatively low intensity. We have therefore expanded the nominal chirp range to 2 GHz to allow both steps to occur near the peak of the pulse. These parameters, 15 ns FWHM pulse and linear chirp of 2 GHz in 28.75 ns, are the benchmark we will use for comparison. Finally, and most importantly, we have removed the restriction of a single linear chirp and allowed for two frequencies as well as an arbitrary temporal variation of the phase (or frequency), with the formation ultimately optimized by LC.

As a first step in attempting to further improve the molecular formation rate, we simply add a second frequency which is chirped synchronously with the first, the idea being that beam 1 would provide the excitation and beam 2 the stimulated emission. Both frequencies are of equal intensity and are linearly chirped with a frequency offset between them of $\Delta/(2\pi)$. The chirp of beam 1 is timed so that it is resonant with the $v'=78$ level at the peak of the pulse. The results are shown in figure 2. Note that in calculating molecular formation rates, both here and in subsequent figures, we average over a two-dimensional Gaussian intensity distribution, since this would typically be the case in experiments. As in [32], we assume a Gaussian intensity distribution of the PA laser (average $1/e^2$ radius $= 119\,\mu$m) and a Gaussian atomic density distribution (average $1/e^2$ radius $= 156\,\mu$m) with a peak value of 5×10^{10} cm^{-3}. The chirps repeat at a rate of 5 MHz. Although this situation exhibits interesting structure as a function of $\Delta/(2\pi)$, including peaks when $\Delta/(2\pi)$ approximately matches both the excited-state splitting (593 MHz) and the final-state binding energy (764 MHz), there is no enhancement relative to the single-beam case, when compared at the same total intensity (solid curve versus dashed curve). On the other hand, if we start with beam 1 (dotted curve) and then add beam 2 (solid curve), thereby doubling the total intensity, we do see a significant enhancement for most values of $\Delta/(2\pi)$.

Figure 3. Molecular formation rate for a single beam, optimized by local control, as a function of peak intensity. The solid curve is using $v'=78$ as the intermediate state, while the dashed curve is for $v'=79$. For comparison, the results for the linear chirp, 2 GHz in 28.75 ns, are shown as the dotted curve.

Figure 4. Solid curve: frequency versus time, as optimized by local control, for the $v'=78$ results of figure 3. The intensity pulse, not shown, is a Gaussian with 15 ns FWHM, centered at 14.4 ns, with a peak intensity of 100 W cm^{-2}. Frequencies are relative to the transition from the zero-energy continuum to $v'=78$. The weighting function used for the local control (see text for details) is shown in the inset.

As a next step, we use a single beam, but incorporate local control of the phase versus time in order to optimize the formation rate. This rate versus intensity is shown in figure 3. Compared to the original linear chirp with a single frequency, LC results in a dramatic enhancement. The temporal variation of the frequency which yields the optimum formation is shown in figure 4. We note that in order to converge, the control must be provided with some guidance. This is done by setting the initial frequency to resonantly excite either $0_g^-(v'=78)$ or $0_g^-(v'=79)$, and then optimizing production of the selected excited state during the first half of the pulse and optimizing production of the target state $(a^3\Sigma_u^+(v''=39))$ during the second half. In the optimization algorithm, the weights of the intermediate (excited) state and the final (target) state in the optimization evolve smoothly during the pulse, as shown in the inset. The optimum step-function behavior for the frequency has a relatively simple interpretation: the frequency stays resonant with the excitation step until the peak of the pulse, optimizing the excited-state population, and then as the weighting shifts, the frequency jumps to the stimulated emission transition, optimizing the transfer. This expected behavior is confirmed in figure 5, where we plot the temporal evolution of the various populations when $v'=78$ is chosen as the intermediate state. Note that these population plots assume a well-defined (peak) intensity and the results are not averaged over intensity. During the first half of the pulse, the $v'=78$ population builds up, while during the second half, a small fraction of this population is stimulated down to $v''=39$. Most of the $v'=78$ population eventually spontaneously decays back into the continuum or into other v'' levels. As seen in figure 5(d), the spontaneous emission contribution to $v''=39$ is very small. We note that $v'=79$ does acquire some population (<5% of that in $v'=78$) when the frequency quickly passes through this resonance during its upward jump.

Figure 5. State populations versus time when the formation is optimized by local control using v'=78 as the intermediate state: (a) v' =78; (b) v'=79; (c) v''=39; (d) v''=39 due to spontaneous emission. The peak intensity is $I = 100$ W cm^{-2} and the 15 ns FWHM pulse is centered at 14.4 ns. Not shown are populations of the 1_g excited states, which have a much smaller maximum of 2.74×10^{-5} in v'=228, and the population of the other bound ground-state levels from spontaneous emission, which approach a total of only 1.13×10^{-9} at long times.

Figure 6. Molecular formation rate versus rounding time τ of the frequency jump. Here the nearly instantaneous jump in frequency resulting from local control optimization is replaced by equation (5). The peak intensity is 100 W cm^{-2}. For comparison, the molecular formation rate optimized by local control (figure 3) is 0.573 (ms^{-1}) at this intensity.
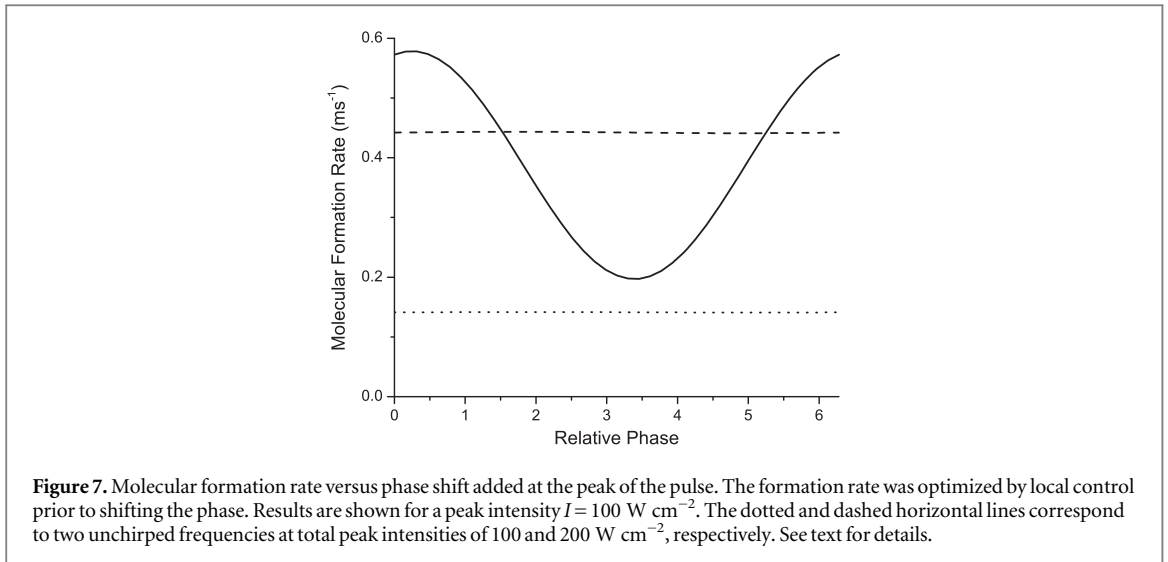
It is evident from figure 4 that LC optimizes the formation rate by an almost instantaneous jump in frequency. An interesting question, especially regarding experimental realization, is how instantaneous this jump needs to be. To address this, we replaced the LC with an analytic variation of the frequency to simulate a rounded step function:

$$f(t) = A * \left(1/2 + (1/\pi) * \arctan\left[\left(t - t_{\text{center}} \right)/\tau \right] \right). \tag{5}$$

The parameter A was chosen to match the jumps in phase and frequency emerging from the LC optimization. The formation rate versus the rounding time τ of the frequency jump is shown in figure 6. The rate falls to 50 % of its peak value for a rounding time of 1.64 ns, which should be experimentally achievable.

The sudden jump in frequency at the peak of the pulse corresponds to a sudden jump in the temporal derivative of the phase. In order to test for coherent effects, we modified the situation described above by simply adding a phase shift during the second half of the pulse. The results, shown in figure 7, confirm that there is

Figure 7. Molecular formation rate versus phase shift added at the peak of the pulse. The formation rate was optimized by local control prior to shifting the phase. Results are shown for a peak intensity $I = 100$ W cm^{-2}. The dotted and dashed horizontal lines correspond to two unchirped frequencies at total peak intensities of 100 and 200 W cm^{-2}, respectively. See text for details.

indeed a strong dependence on this phase. The maximum at approximately zero phase shift is simply a consequence of the fact that the phase has already been optimized by the LC. Since the LC-optimized frequency variation (figure 4) is a jump between the upward transition and the downward transition, it is useful to compare these results with those obtained by simply having both resonant frequencies present throughout the pulse, as shown by the horizontal lines in figure 7. The lower (dotted) line is for the same total peak intensity (100 W cm^{-2}) as for the solid curve, split evenly between the two frequencies. The upper (dashed) line is for a peak intensity of 100 W cm^{-2} for each frequency. Interestingly, in both cases, the pulse for which the frequency jumps optimally between the two values outperforms the pulse where both frequencies are continuously present. We have also calculated the formation rate when the two frequencies are applied as separate Gaussian pulses delayed by one pulse width (15 ns). For the intuitive pulse order, where the excitation from the continuum to $v'=78$ is applied before the stimulated emission from $v'=78$ to $v''=39$, we find a slight improvement relative to overlapping pulses (dashed and dotted lines in figure 7): 0.16 versus 0.14 for a total peak intensity of 100 W cm^{-2}; and 0.48 versus 0.44 for a total peak intensity of 200 W cm^{-2}. Using instead the counterintuitive pulse order, which corresponds to the case of STIRAP [39], the formation rate is reduced by approximately one order of magnitude. This is not surprising because STIRAP is an adiabatic process and here we are far from the adiabatic regime due to the combination of short pulse, low intensity, and relatively weak free-to-bound and bound-to-bound transitions.

Encouraged by both the enhancement provided by guided LC (see figure 4 inset), and the evidence for coherence seen in the dependence on phase shift, we investigated the possibility of further enhancement by taking advantage of two intermediate states. To do this, we set the initial frequency to be midway between the v' $=78$ and $v'=79$ intermediate states and use LC to optimize the $v'=78$ population. Note that because a one-photon transition is not sensitive to phase, the detuning remains at its initial value during this initial time interval. Near the peak of the pulse, we then switch to optimizing the $v''=39$ target state. The weighting is the same as that in the insert to figure 4. The result is an improved target state population, 5.60×10^{-8}, compared to the value of 3.20×10^{-8} obtained with a single intermediate state (figure 5(c)) at the same intensity of 100 W cm^{-2}. Interestingly, this enhancement is accomplished while significantly suppressing the intermediate state populations by being off-resonant, 1.98×10^{-4} in $v'=78$ and 1.99×10^{-4} in $v'=79$, compared to the value of 4.23×10^{-3} in the resonant single-intermediate-state case (figure 5(a)). However, the optimizing phase pattern is very complicated, exhibiting instantaneous rates of change of frequency up to $\sim$100 GHz ns^{-1}. We show in figure 8 a false-color plot of a sliding-window fast Fourier transform (FFT) of the resulting pulse. The various frequencies present in the FFT correspond to transitions in the system, as indicated by the arrows. It is seen that multiple intermediate states are populated as a consequence of the rapid phase variations. This less obvious optimization shows the power of LC. However, such a complicated phase variation does not allow a simple interpretation, and more importantly, is not experimentally feasible due to the rapid phase variations and the dependence of the details on intensity.

As a final step, we combine the two-frequency scheme and guided LC, aiming to take advantage of quantum interference between paths. As described above and displayed in figures 3–5, we use LC to optimize the molecular formation, going through the $v'=78$ excited state. We then do the same but going through the $v'=79$ excited state. The optimizing frequency versus time for these two cases are essentially the same except for a constant offset corresponding to the frequency difference between $v'=79$ and $v'=78$. We then combine these two
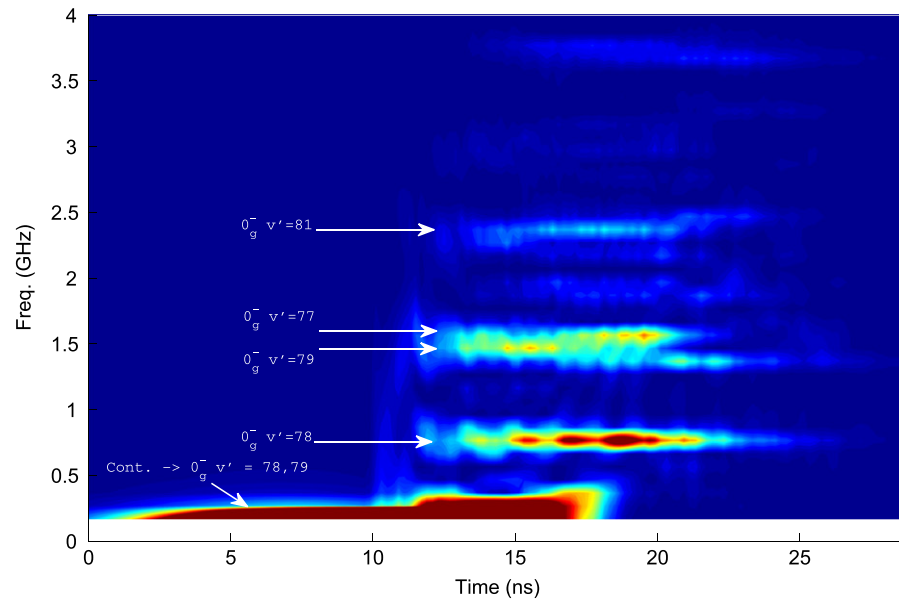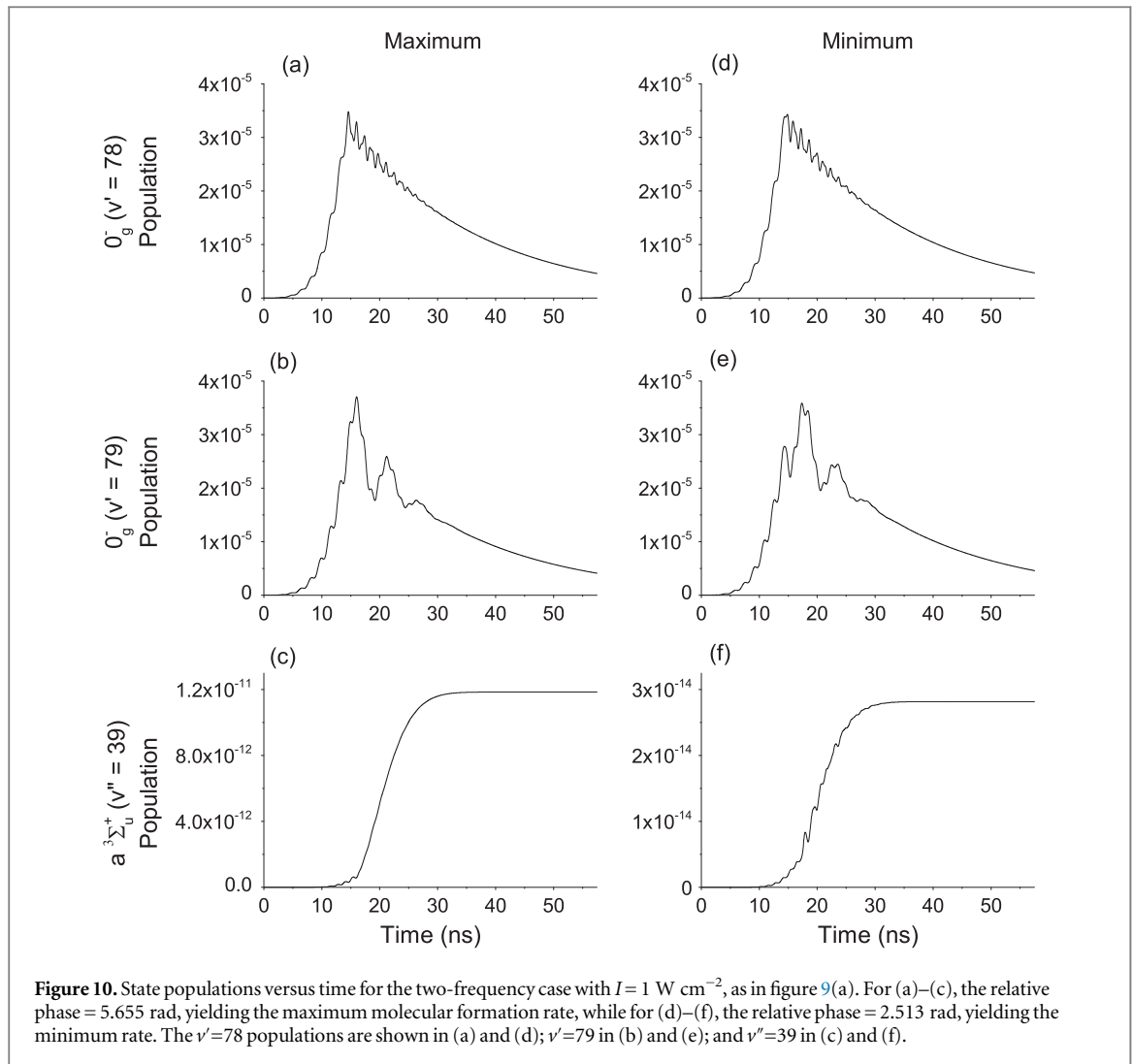
Figure 8. Sliding-window FFT of the Gaussian pulse with the optimizing phase pattern resulting from local control with two intermediate states. The width of the sliding window is 15 ns and the 15 ns FWHM intensity pulse is centered at 14.4 ns. Only absolute values of relative frequency are shown, with zero frequency corresponding to the initial frequency. This is located midway between the transitions from the continuum to 0_g^- (v'=78 and 79), which are separated by 593 MHz. Various 0_g^- (v')$\rightarrow a^3\Sigma_u^+$ (v''=39) downward transition frequencies are indicated with horizontal arrows, while the upward transitions from the continuum to v'=78 and 79 are located within the bright band below 300 MHz.
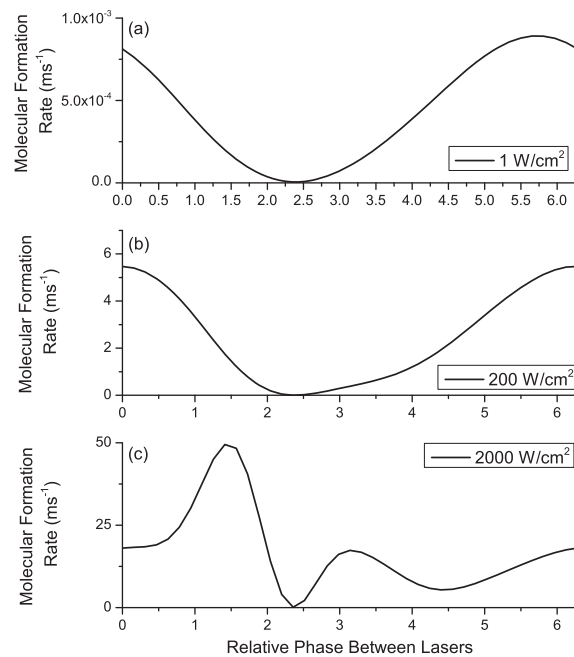
Figure 9. Molecular formation rate for the case of two frequencies, initially tuned to the v'=78 and v'=79 excited states, where the temporal evolutions have been separately optimized by local control. Plotted is the formation rate when these two fields, with an added relative phase, are simultaneously applied. Results are shown for several total peak intensities: (a) $I = 1$ W cm^{-2}; (b) $I = 200$ W cm^{-2}; (c) $I = 2000$ W cm^{-2}.
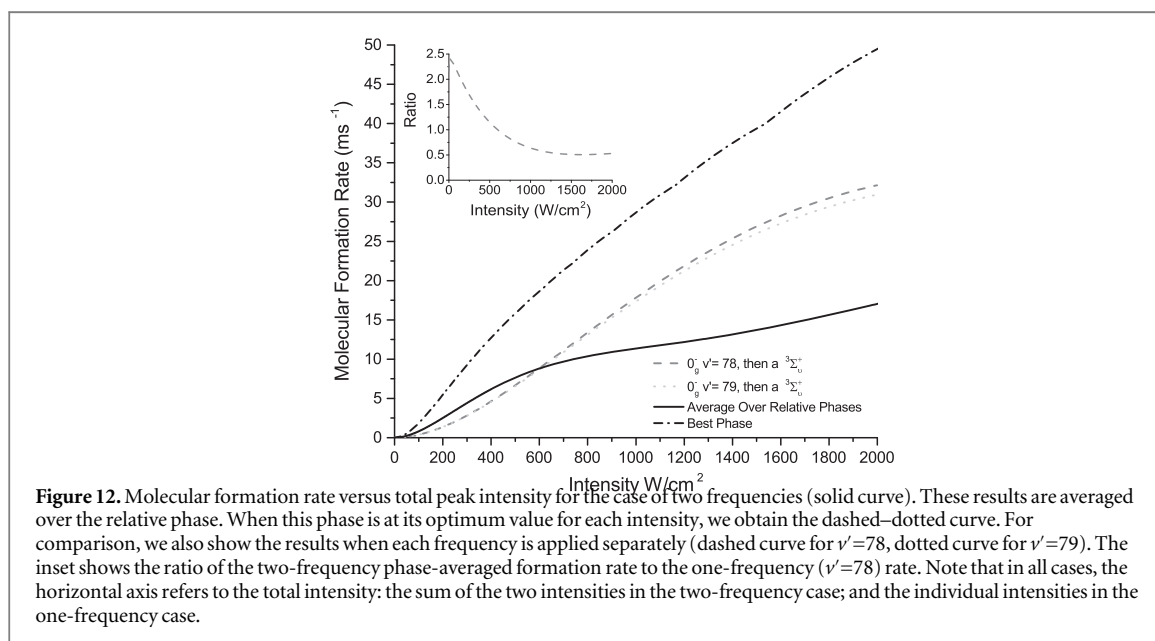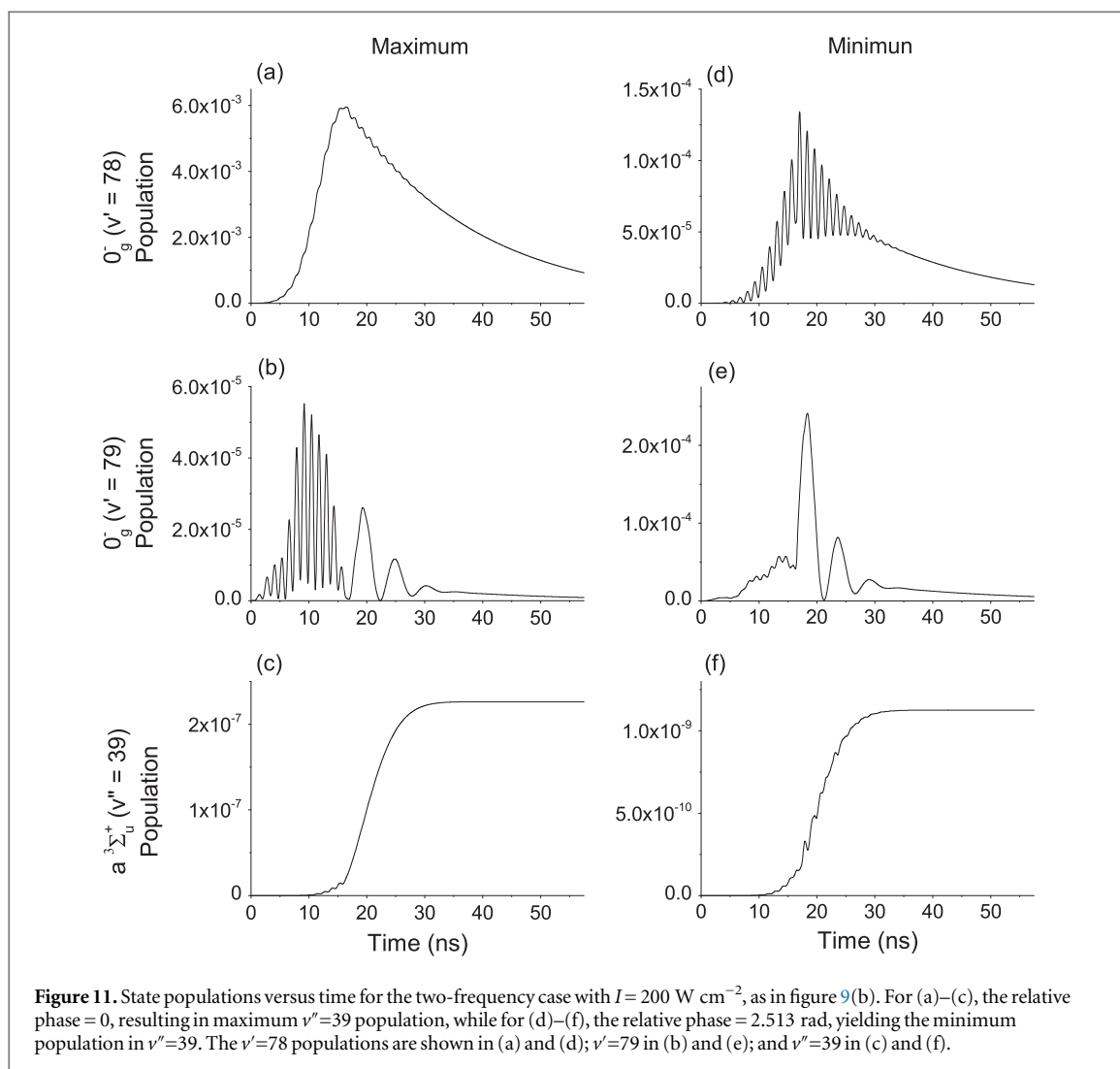
equal-intensity beams, having separately optimized their individual formation rates, and adjust their relative phase. The results, shown in figure 9 for several different intensities, exhibit what appears to be almost complete constructive and destructive interference. At first glance, this is not unexpected. We are going from the initial state to the final state via two paths of almost equal amplitude. However, when we consider that the initial state is a continuum and that the total rate of spontaneous emission is not negligible, the degree of contrast is somewhat surprising. To understand the details of the interference, we examine the various state populations for the two relative phases which give maximum and minimum molecular formation rates. We first explore the case of low

Figure 10. State populations versus time for the two-frequency case with $I = 1$ W cm^{-2}, as in figure 9(a). For (a)–(c), the relative phase = 5.655 rad, yielding the maximum molecular formation rate, while for (d)–(f), the relative phase = 2.513 rad, yielding the minimum rate. The $v'=78$ populations are shown in (a) and (d); $v'=79$ in (b) and (e); and $v''=39$ in (c) and (f).

intensity, 1 W cm^{-2} (total intensity, shared between the two beams), which should be in the perturbative limit. We see in figure 10 that the populations in the intermediate states, $v'=78$ and $v'=79$, are quite similar. For the optimum relative phase (5.655 rad), the two paths through these two intermediate states interfere constructively, yielding a maximum target state ($v''=39$) population. For a relative phase of 2.513 rad, the intermediate state populations are still similar, but the time dependence is slightly shifted in time, causing destructive interference in the target state and reducing the yield by more than two orders of magnitude.

Switching now to a higher total intensity of 200 W cm^{-2}, on the order of what has been realized experimentally [32], we see a similar contrast in the final yield. However, examining the state populations, as shown in figure 11, we find that the manifestations of the interference are quite different. Comparing the cases corresponding to the maximum (relative phase = 0) and and the minimum (relative phase = 2.513 rad) in figure 9(b), we see a significant change in not only the final state ($v''=39$) population, but also in the intermediate state ($v'=78$ and $v'=79$) populations. It appears that the key ingredient for destructive interference is having approximately equal intermediate state populations, while for maximum target state population, these intermediate state populations are very different. Comparing figures 11(a) and (d), we see that the $v'=78$ population is reduced by a factor of ~40 simply by changing the relative phase of the light driving the transition to and from $v'=79$. Clearly there is a strong interaction between the two arms of this 'interferometer'. The nontrivial nature of the interference is reinforced by the complicated phase dependence of the formation rate at higher intensities, as shown in figure 9(c).

If we average the formation rate over the relative phase, as shown in figure 12, we find that at low intensities, there is still significant enhancement over the case of the single beam with LC, when comparing at the same total intensity. This is encouraging because it implies that the relative phase does not need to be stabilized in order to

Figure 11. State populations versus time for the two-frequency case with $I = 200$ W cm^{-2}, as in figure 9(b). For (a)–(c), the relative phase = 0, resulting in maximum $v''=39$ population, while for (d)–(f), the relative phase = 2.513 rad, yielding the minimum population in $v''=39$. The $v'=78$ populations are shown in (a) and (d); $v'=79$ in (b) and (e); and $v''=39$ in (c) and (f).

Figure 12. Molecular formation rate versus total peak intensity for the case of two frequencies (solid curve). These results are averaged over the relative phase. When this phase is at its optimum value for each intensity, we obtain the dashed–dotted curve. For comparison, we also show the results when each frequency is applied separately (dashed curve for $v'=78$, dotted curve for $v'=79$). The inset shows the ratio of the two-frequency phase-averaged formation rate to the one-frequency ($v'=78$) rate. Note that in all cases, the horizontal axis refers to the total intensity: the sum of the two intensities in the two-frequency case; and the individual intensities in the one-frequency case.

gain some enhancement. Of course, if the relative phase is stabilized at its optimum value, even more enhancement, by roughly a factor of two, is realized.

4. Conclusion

We have examined the possibility of enhancing photoassociative ultracold molecule formation using LC of the phase. We find that LC does indeed outperform a simple linear chirp, and that the optimum frequency variation corresponds to a nearly instantaneous jump from the continuum-to-excited-state transition to the excited-state-to-bound-state transition. The dependence on phase verifies that the process has a significant coherent aspect. We can improve the formation rate even further by combining two LC-optimized beams which drive transitions to and from different excited states. Surprisingly, even after averaging over relative phase, we find, at the same total intensity, an enhancement relative to the single-beam case under some conditions. We can take advantage of the strong dependence on this relative phase and obtain an additional enhancement at a fixed optimal phase. The explored values for intensity, pulse width, and frequency variation should be experimentally realizable with nanosecond-time-scale pulse shaping techniques.

Interesting avenues for future investigations include incorporation of LC of not only the phase, as we have done here, but also the amplitude, in the optimization algorithm. Also, in experiments, an important practical aspect is that a sequence of chirped pulses is typically used. Therefore, the photodestruction of molecules by a subsequent pulse must be considered [32]. Simultaneous optimization of formation and minimization of this destruction would therefore be a useful endeavor. Finally, it would be useful to compare the results of LC to more global types of control such as genetic algorithms.

Acknowledgments

References

[1] Krems R V, Stwalley W C and Friedrich B (ed) 2009 *Cold Molecules: Theory, Experiment, Applications* (Boca Raton, FL: CRC Press)
[2] Thorsheim H, Weiner J and Julienne P 1987 *Phys. Rev. Lett.* **58** 2420
[3] Stwalley W C and Wang H 1999 *J. Mol. Spectrosc.* **195** 194–228
[4] Jones K M, Tiesinga E, Lett P D and Julienne P S 2006 *Rev. Mod. Phys.* **78** 483
[5] Stwalley W C, Gould P L and Eyler E E 2009 *Ultracold Molecule Formation by Photoassociation* p 169 ch 5 in Krems *et al* [1]
[6] Koch C P and Shapiro M 2012 *Chem. Rev.* **112** 4928–48
[7] Rice S A 1992 *Science* **258** 412–3
[8] Brumer P and Shapiro M 1992 *Annu. Rev. Phys. Chem.* **43** 257–82
[9] Vala J, Dulieu O, Masnou-Seeuws F, Pillet P and Kosloff R 2000 *Phys. Rev. A* **63** 013412
[10] Luc-Koenig E, Kosloff R, Masnou-Seeuws F and Vatasescu M 2004 *Phys. Rev. A* **70** 033414
[11] Luc-Koenig E, Vatasescu M and Masnou-Seeuws F 2004 *Eur. Phys. J. D-At. Mol. Opt. Plasma Phys.* **31** 239–62
[12] Koch C P, Kosloff R and Masnou-Seeuws F 2006 *Phys. Rev. A* **73** 043409
[13] Poschinger U, Salzmann W, Wester R, Weidemüller M, Koch C P and Kosloff R 2006 *J. Phys. B: At. Mol. Phys.* **39** S1001
[14] Koch C P, Kosloff R, Luc-Koenig E, Masnou-Seeuws F and Crubellier A 2006 *J. Phys. B: At. Mol. Phys.* **39** S1017
[15] Brown B L and Walmsley I A 2006 *J. Phys. B: At. Mol. Phys.* **39** S1055
[16] Koch C P, Luc-Koenig E and Masnou-Seeuws F 2006 *Phys. Rev. A* **73** 033408
[17] Mur-Petit J, Luc-Koenig E and Masnou-Seeuws F 2007 *Phys. Rev. A* **75** 061404
[18] Kallush S, Kosloff R and Masnou-Seeuws F 2007 *Phys. Rev. A* **75** 043404
[19] Kallush S and Kosloff R 2008 *Phys. Rev. A* **77** 023421
[20] Koch C P and Moszyński R 2008 *Phys. Rev. A* **78** 043417
[21] Koch C P, Ndong M and Kosloff R 2009 *Faraday Discuss.* **142** 389–402
[22] Koch C P, Palao J P, Kosloff R and Masnou-Seeuws F 2004 *Phys. Rev. A* **70** 013402
[23] Kallush S and Kosloff R 2007 *Phys. Rev. A* **76** 053408
[24] Viteau M, Chotia A, Allegrini M, Bouloufa N, Dulieu O, Comparat D and Pillet P 2008 *Science* **321** 232–4
[25] Salzmann W *et al* 2006 *Phys. Rev. A* **73** 023414
[26] Brown B L, Dicks A J and Walmsley I A 2006 *Phys. Rev. Lett.* **96** 173002
[27] Engel V, Meier C and Tannor D J 2009 *Adv. Chem. Phys.* **141** 29–101
[28] Kosloff R, Rice S A, Gaspard P, Tersigni S and Tannor D 1989 *Chem. Phys.* **139** 201–20
[29] Palao J P and Kosloff R 2003 *Phys. Rev. A* **68** 062308
[30] Tannor D J 2007 *Introduction to Quantum Mechanics: A Time-Dependent Perspective*
[31] Judson R S and Rabitz H 1992 *Phys. Rev. Lett.* **68** 1500
[32] Carini J L, Pechkis J A, Rogers C E, Gould P L, Kallush S and Kosloff R 2013 *Phys. Rev. A* **87** 011401 (R)
[33] Kemmann M, Mistrik I, Nussmann S, Helm H, Williams C J and Julienne P S 2004 *Phys. Rev. A* **69** 022715
[34] Kallush S and Kosloff R 2006 *Chem. Phys. Lett.* **433** 221–7
[35] Carini J, Pechkis J, Rogers C III, Gould P, Kallush S and Kosloff R 2012 *Phys. Rev. A* **85** 013424
[36] Gutterres R, Amiot C, Fioretti A, Gabbanini C, Mazzoni M and Dulieu O 2002 *Phys. Rev. A* **66** 024502

[37] Julienne P and Vigué J 1991 *Phys. Rev. A* **44** 4464
[38] Koch C P and Kosloff R 2010 *Phys. Rev. A* **81** 063426
[39] Vitanov N V, Halfmann T, Shore B W and Bergmann K 2001 *Annu. Rev. Phys. Chem.* **52** 763–809